CrystEngComm

RSC Publishing

PAPER

View Article Online
View Journal | View Issue

Cite this: *CrystEngComm*, 2013, **15**, 2966

Alkali metal ion assisted synthesis of faceted anatase TiO_2†

Min-Han Yang,[a] Po-Chin Chen,[a] Min-Chiao Tsai,[a] Ting-Ting Chen,[a] I-Chun Chang,[a] Hsin-Tien Chiu[b] and Chi-Young Lee*[a]

Received 4th December 2012,
Accepted 1st February 2013

DOI: 10.1039/c3ce26965e

www.rsc.org/crystengcomm

This work reports on a simple hydrothermal method for tuning the shape and exposed face of TiO_2 nanocrystal by using sodium titanate as a precursor in the presence of different alkali metal ion salts. The {101}-exposed anatase TiO_2 was synthesized in lithium salt solution. The formation of anatase TiO_2 with exposed high-index {301} facet, obtained in the presence of sodium ions, has never before been reported upon. When the reaction proceeded in potassium salt solution, the obtained anatase TiO_2 with a high aspect ratio was elongated in the <001> direction. Anatase TiO_2 with a high aspect ratio was obtained in hydrothermal process in the presence of low charge density high atomic number alkali metal ions, which were not easily absorbed by the {001} planes of anatase, so the growth along this direction was not restrained. The photodegradation of methylene blue, assisted by anatase TiO_2 with various exposed faces reveals that the photoactivity of anatase {101} planes is larger than that of {301} planes.

Introduction

Recently, crystal facet engineering of semiconductor materials has attracted considerable attention because such facet engineering can be utilized to alter their physicochemical properties.[1] The atomic arrangement and coordination at the surface strongly influences the reactivity.[2] Therefore, the active surface of semiconductor materials affects the performance of various applications in which they are utilized, such as catalysis,[3,4] sensors,[5] solar cells[6] and batteries.[7]

Titanium dioxide is one of the most important semiconductor materials.[8–10] To control the shape and the exposed surface thereof, two main strategies are utilized. These are the use of an organic capping agent[11] and the adsorption of anions[12–14] on a particular surface of the TiO_2. T. Do *et al.* used a solvothermal method to control the ratio of oleic acid to oleylamine to realize spherical, rhombic and truncated rhombic shapes of anatase TiO_2.[15] Hydrogen fluoride has been used to produce anatase TiO_2 with a large proportion of {001} exposed. The tendency of the {001} facet to adsorb fluoride ions results in anisotropic growth and {001}-exposed anatase TiO_2.[12,16] The aforementioned methods are most limited by the facts that only the low-index facets of anatase TiO_2 such as {100}, {101} and {001} are predominantly exposed. Anatase TiO_2 with high-index exposed facets, which have unique surface atomic structures, potentially have various applications. However, high-index crystal facets with high surface energies being thermodynamically unstable tend to disappear, making the synthesis of TiO_2 with exposed high-index surfaces difficult. Recently, H. Yang *et al.* synthesized anatase TiO_2 with exposed high-index {105} and {107} facets at a high temperature (1000 °C).[17] X. Lou *et al.* synthesized asymmetric anatase TiO_2 with exposed (201) and (401) facets using a solvothermal method.[18] These approaches require the use of highly toxic chemicals or the production of organic waste.

This work develops a simple hydrothermal approach to tailor the shape of TiO_2. Elongated anatase TiO_2 and anatase TiO_2 with {101} and {301} exposed were synthesized using sodium titanate as precursor in the presence of various alkali metal ion salts. The photoactivities of anatase TiO_2 with various exposed faces were investigated.

Experimental section

Preparation of sodium titanate

Sodium titanate was synthesized by adding commercial TiO_2 (Riedel-de-Haën) to a 10 M aqueous NaOH.[19] The mixture was refluxed at 150 °C for 48 h. The obtained powder was washed in D.I. water to remove the unreacted NaOH. After filtration and drying at 50 °C, sodium titanate was collected as the precursor.

[a]*Department of Materials Science and Engineering, National Tsing Hua University, Hsinchu, Taiwan, 30013, R. O. C.. E-mail: cylee@mx.nthu.edu.tw; Fax: +886 3571 3113; Tel: +886 3572 8692*

[b]*Department of Applied Chemistry, National Chiao Tung University, Hsinchu, Taiwan, 300, R. O. C.. E-mail: htchiu@cc.nctu.edu.tw; Fax: +886 3571 3113; Tel: +886 3513 1514*

† Electronic supplementary information (ESI) available. See DOI: 10.1039/c3ce26965e

Preparation of anatase TiO_2

A 0.5 g mass of sodium titanate was added to 30 ml DI water under ultrasonication. To understand the effect of salts on anatase TiO_2 growth, alkali metal ion salts (0.075 M LiCl, 0.25 M NaCl and 0.25 M KCl, respectively) were added to the mixture. To confirm the findings, other salts (LiBr, NaBr and KI, respectively) were added to the mixture in separate experiments. The solution was transferred to a Teflon-lined autoclave and heated to 200 °C for 20 h. After the hydrothermal process, the product was washed with DI water and dried in an oven at 50 °C. The TiO_2 products were separately obtained using LiCl, NaCl, KCl and a mixture of LiCl and KCl (Li : K = 10 : 1) that were denoted as B-TiO_2 (bipyramidal), S-TiO_2 (spindle-shaped), N1-TiO_2 (needle-like) and O-TiO_2 (olive-like) respectively. The predominantly {100}-exposed anatase TiO_2 was synthesized by the method in the literature[20] and was denoted as N2-TiO_2 (needle-like).

Material characterization

Field emission scanning electron microscopy (FE-SEM, JSE-6500F field emission SEM) was used to characterize the surface morphologies of the anatase TiO_2 materials. High-resolution morphology and microstructure of the anatase TiO_2 were examined using transmission electron microscopy (JEM-2010 and JEM-3000F). Phase detection analysis was performed by using XRD patterns (Brucker D8-advanced with Cu Kα radiation λ = 1.5405981 Å).

Photocatalytic experiment

The light source for photocatalysis was a 180 W Xe bulb from Osram, and the temperature was maintained at 296 K using a water cooling jacket. The target pollutant was methylene blue. A 0.01 g mass of catalyst powder was dispersed to a concentration of 25 ppm in methylene blue solution. After the absorption had stabilized, it was illuminated from the top with magnetic stirring. Samples with a volume of 1 mL were removed every five minutes, filtered through a 0.2 μm filter, and diluted by adding 1.5 ml D.I. water. The filtrate was then analyzed by obtaining its UV-visible spectrum (AvaSpec-2048UVspectrum) to determine the target concentration. The pseudo-first-order rate constant, k, was calculated using the equation, $k = -[\ln(C/C_0)]/\Delta t$, where C represents the final concentration; C_0 is the initial concentration, and Δt is time.

Results and discussion

Shape-tailored TiO_2 was synthesized using a hydrothermal process with sodium titanate as the precursor in the aqueous solution that was separately mixed with different alkali metal ion salts. Bipyramidal (B-TiO_2), spindle-shaped (S-TiO_2) and needle-like (N1-TiO_2) titanium dioxides were obtained when LiCl, NaCl and KCl were added in the reaction solution, respectively, as presented in Fig. 1A–C. The sizes of B-TiO_2 with an aspect ratio of approximate 2.3 typically ranged from 50 to 120 nm. The aspect ratio of S-TiO_2 was 4.3 and the length of the long axis ranged from 150 to 350 nm, whereas the corresponding values for N1-TiO_2 were 7.9 and usually above

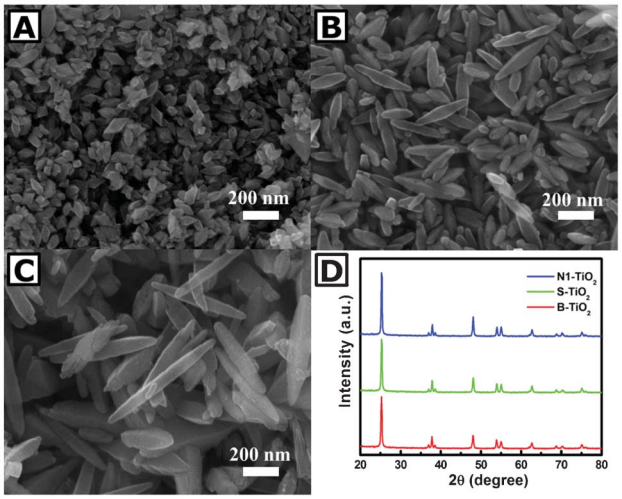

Fig. 1 FESEM images of anatase TiO_2 obtained in the presence of various alkali metal ion salts in hydrothermal process. (A) B-TiO_2 obtained in LiCl solution. (B) S-TiO_2 obtained in NaCl solution. (C) N1-TiO_2 obtained in KCl solution. (D) XRD patterns of anatase TiO_2.

500 nm, respectively. Although the obtained TiO_2 powders had very different shapes, the XRD patterns (Fig. 1D) of the three samples were all consistent with anatase phase TiO_2 (JCPDS file No. 89-4921, $I4_1/amd$, $a = b$ = 0.3777 nm and c = 0.9501 nm).

Fig. 2–4 presents the TEM morphological analyses of variously shaped anatase TiO_2. Fig. 2B presents an HRTEM image of the tip of B-TiO_2 in Fig. 2A. The fringes from the (101), ($\bar{1}$01), and (002) planes reveal d spacings of 0.35, 0.35, and 0.48 nm, respectively. The (101) and ($\bar{1}$01) planes are parallel to the edges of B-TiO_2, suggesting that the circumferential faces of B-TiO_2 are {101} planes.[21]

The SAED in Fig. 3B shows a spot pattern of spindle-shaped TiO_2, revealing the single crystalline structure of the samples. The patterns can be indexed as the [010] zone axis of anatase TiO_2. The pattern reveals that the apparent elongated direction of S-TiO_2 is <001>, and the exposed surface of S-TiO_2 can be determined from the (301) and (30$\bar{1}$) spots of the electron diffraction pattern. Fig. 3C and D display HRTEM images of the regions that are outlined by blue and red squares in Fig. 3A, respectively. The included angle between the long edge of the spindle and (001) is approximately 82.5°, as shown in

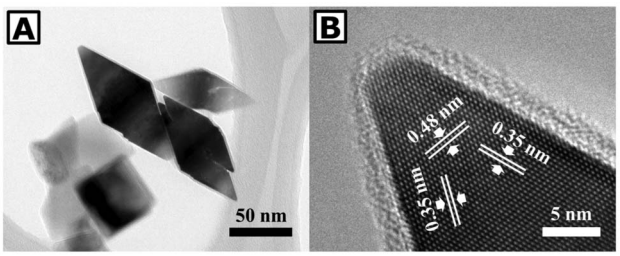

Fig. 2 (A) TEM and (B) HRTEM images of B-TiO_2.

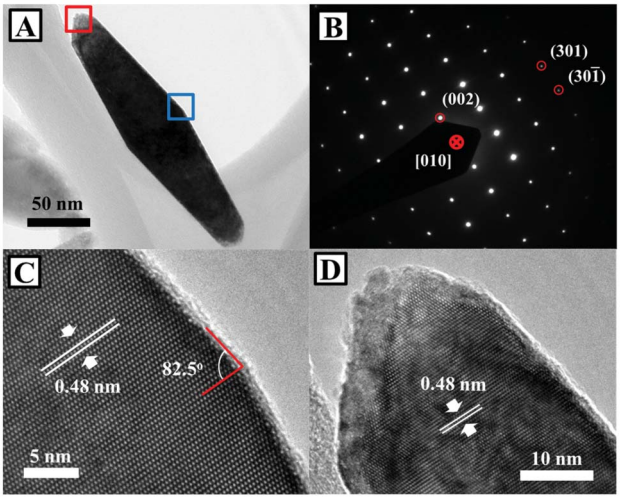

Fig. 3 TEM analyses of S-TiO_2: (A) TEM image (B) selected area electron diffraction pattern. HRTEM images of region in (C) blue and (D) red squares in (A).

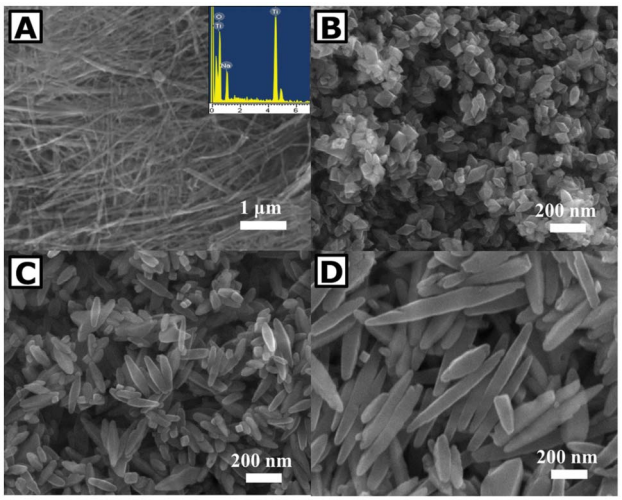

Fig. 5 FESEM images of (A) sodium titanate, (B) bipyramidal shaped TiO_2 obtained in LiCl solution, (C) spindle-shaped TiO_2 obtained in NaCl solution and (D) needle-like shaped TiO_2 obtained in KCl solution. Inset in (A) presents the EDS analysis of sodium titanate.

Fig. 3C, which is consistent with the calculated dihedral angle, 82.45°, between plane (301) and plane (001) of anatase. The *d* spacing, 0.48 nm, of anatase (002) is observed in Fig. 3C and D, and the end of the S-TiO_2 is not a clear cut face. Observations reveal that the circumferential faces of the S-TiO_2 are {301} planes. To the best of our knowledge, anatase TiO_2 crystals with predominantly exposed high-index {301} facets have never been reported upon.

Fig. 4A presents N1-TiO_2 with a high aspect ratio. Since the included angle between the long edge and (001) is approximately 82.5°, which is consistent with the dihedral angle between the (301) and (001) planes, 82.45°, the {301} exposed surface is observed at the ends of N1-TiO_2 in Fig. 4B. The *d* spacing, 0.48 nm, was obtained from Fig. 4B–D, consistent with the (002) anatase plane and suggesting that the direction of elongation is <001>. However, in the middle part of the needle, the surface with no specific preferred exposed face appears very rough.[22]

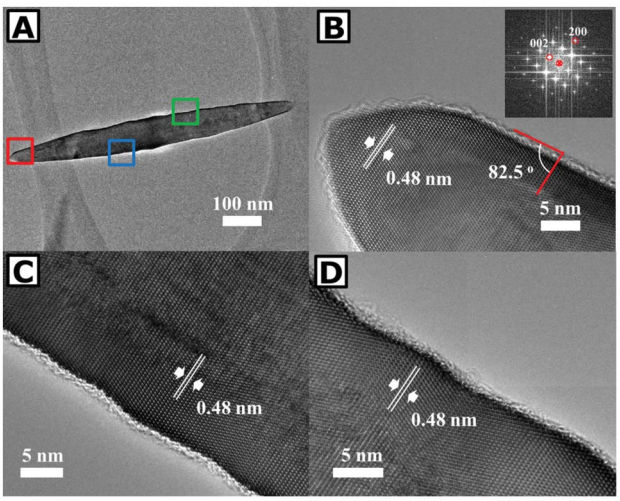

Fig. 4 TEM analyses of N1-TiO_2: (A) TEM image. HRTEM images of region that is marked in (B) red, (C) blue and (D) green squares in (A). Inset in (B) presents Fourier-transformed image of N1-TiO_2 end part.

To determine the variation of the shape of TiO_2 with the alkali metal salt additives that are used in synthetic hydrothermal processes, hydrothermal reactions of sodium titanate in LiBr, NaBr and KI solutions and in only DI water were performed. When sodium titanate was heated in only D.I. water in a hydrothermal process, the {301}-exposed spindle anatase was the major product (Fig. S1, ESI†). It may be attributed to Na^+ cations released from sodium titanate (Fig. 5A). Additionally, the shapes of the anatase TiO_2 that were obtained in LiBr, NaBr and KI solutions were consistent with those of TiO_2 that were obtained in LiCl, NaCl and KCl solutions, respectively, as shown in Fig. 5B–D. Based on the above observations, alkali metal ions in the hydrothermal solution are the major cause of the variation in shape of TiO_2. When Li^+ cations were present in the reaction solution, {101} plane-exposed bipyramidal B-TiO_2 was the major product. When Na^+ cations were present in the reaction solution, {301} plane-exposed spindle-shaped S-TiO_2 was the major product. When large K^+ cations were present in the reaction solution, needle-like N1-TiO_2 with a {301} exposed tip and a <001> long axis was the major product.

The growth of a particular shaped crystal was obtained by the anisotropic stacking of different basis planes.[23,24] An anatase crystal is a tetragonal system (space group $I4_1/amd$) and the stacking characteristic of (100) equals that of (010). To elucidate this anisotropic growth, a simulation was performed to elucidate the relationship between TiO_2 shape and stacking rates using the WinXMorph crystal morphology builder.[25] Fig. 6 plots the growth rate of particularly shaped TiO_2. The growth rate ratio of {001}/{100} in B-TiO_2 was around 2.2,

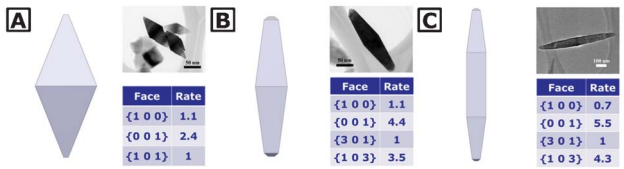

Fig. 6 Growth rate of (A) B-TiO_2, (B) S-TiO_2 and (C) N1-TiO_2, simulated using WinXMorph crystal morphology builder.

whereas those in S-TiO_2 and N1-TiO_2 were around 4 and 7.9, respectively. The growth rate ratio of {001}/{100} planes was strongly coupled to the aspect ratio of the powders, and rapid growth along the <001> direction increased the aspect ratio, resulting in the long TiO_2. The slow stacking directions determined the exposed faces of the particles. In B-TiO_2, the slow stacking direction was <101>, so the major product had a {101} plane-exposed bipyramidal structure; in S-TiO_2, the slow stacking direction was <301>, yielding spindle-shaped powder with {301} as the major exposed plane; in N1-TiO_2, the slow stacking directions were <100> and <301>, yielding needle-like structures that grew along the <001> direction with {301} as the major exposed plane at the ends. Based on the above observations, the restriction of the growth in the <001> direction varied with the alkali metal ion species in solution. In the solution that contained Li^+ cations, growth in the <001> direction was seriously restricted, yielding small particles with {101} planes exposed. In the solution that contained K^+ cations, the growth in the <001> direction was restricted very weakly, yielding long particles along the <001> axis.

A detailed investigation of Ti^{4+} and O^{2-} packing in anatase TiO_2 revealed that the distributions of Ti^{4+} and O^{2-} on {001} and {100} planes differed, resulting in different charge distributions on these planes. In Fig. 7A, Ti^{4+} and O^{2-} ions are present on the {100} planes. However on the {001} planes, Ti^{4+} ions are present on the {001}, whereas O^{2-} ions are present slightly beneath the {001} layers, as shown in the inset of Fig. 7B, thus causing the {001} planes to become partially positively charged. As in an alkali metal ion assisted TiO_2 growth reaction, positively charged alkali metal ions are attracted by the negatively charged O^{2-} ions on the surface of the TiO_2 particles, limiting its growth. The charge density of the alkali metal ions herein decreases in the order $Li^+ > Na^+ > K^+$.[26] The alkali metal ion, Li^+, with the largest charge density was attracted by the O^{2-} ions both on the {100} planes and under the {001} planes, greatly restraining the growth in both directions, leading to the production of small particles with a low aspect ratio. In contrast, the alkali metal ion, K^+, with a small charge density was easily attracted by O^{2-} ions on the {100} planes, but by the O^{2-} ions under the {001} planes weakly, so the growth in the <100> direction was seriously restrained, resulting in the production of needle-shaped particles along the <001> direction with a high aspect ratio (Fig. 7C–E).

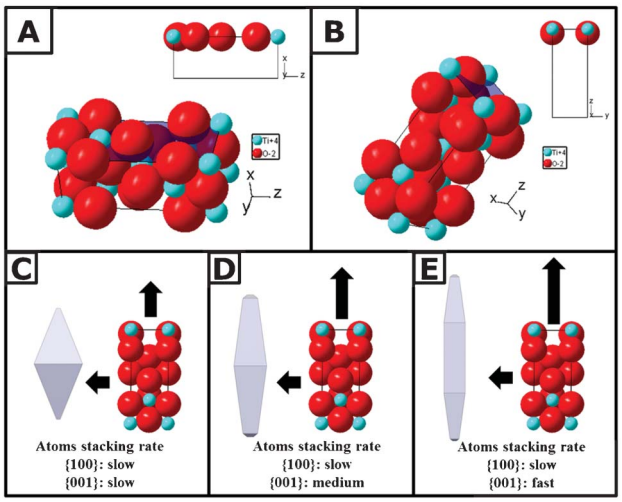

Fig. 7 Atomic arrangement of anatase unit cell: (A) (100) plane, (B) (001) plane. The anisotropic atom stacking on {100} and {001} plane of different alkali metal ion salt solution (C) B-TiO_2 in Li^+ ion salt solution. (D) S-TiO_2 in Na^+ ion salt solution. (E) N1-TiO_2 in K^+ ion salt solution

To understand the restriction of the growth of anatase TiO_2 in different directions upon the addition of Li^+, Na^+ and K^+ in the reaction, the mixed salts were used in the hydrothermal process. Bipyramidal anatase TiO_2 (Fig. S2, ESI†) was obtained as the major product when 0.075 M LiCl and 0.25 M KCl were added, even though the concentration of potassium ion was three times higher that of lithium ions. As the concentration of LiCl was reduced to 0.025 M while that of KCl was maintained at 0.25 M (K : Li = 10 : 1), olive-shaped anatase TiO_2 (O-TiO_2) with an aspect ratio of 3.5 was obtained, as displayed in Fig. 8A and B. The SAED in the inset in Fig. 8B demonstrates that the long axis is along the <001> direction. Fig. 8C presents the exposure of a {101} surface at the end of O-TiO_2, and the angle,

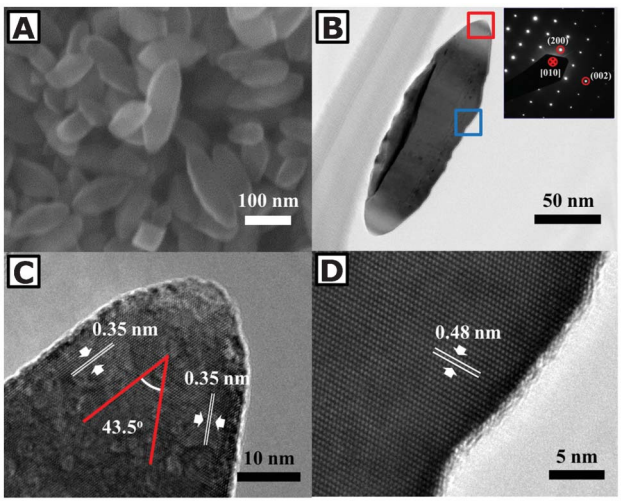

Fig. 8 EM analyses of O-TiO_2: (A) SEM image, (B) TEM image. HRTEM images of region that is marked in (C) red and (D) blue in (B). Inset in (B) presents electron diffraction pattern.

43.5°, is consistent with the dihedral angle (43.39°) between (101) and ($\bar{1}$01) planes. Fig. 8D shows no preferred exposed surface on the body of O-TiO_2. Even when considerable KCl (0.25 M) was utilized during the reaction, Li^+ (0.075 M) plays a major role in the formation of bipyramidal TiO_2, whereas reducing the concentration of Li^+ to 0.025 M, leads to the elongation in the particle size with {101} exposed tip. Thus indicating that lithium ions significantly affect the anatase shape. At very low concentrations of lithium, potassium ions elongated the particle size in the <001> direction, thus yielding O-TiO_2 as the long axis but still with a {101} exposed tip.

According to an earlier investigation, the two common methods for controlling the shape of TiO_2 particles are to use an organic capping agent[11,15,27,28] and to adsorb anions[12–14] onto particular planes of the particles. Spherical to rod-like titanium dioxides were obtained by adjusting the ratio of oleic acid/oleylamine in a solvothermal reaction.[15] Introducing fluoride ions into the acidic solution substantially increased the absorption of anions on the {001} planes of TiO_2, forming the {001}-exposed anatase TiO_2.[12,29] However, under the reaction conditions herein, the pH value was around 12. Alkali metal ions are suggested to play important roles in the shape tailoring reaction of anatase during the experiments. To the best of our knowledge, this work is the first in which the morphologies of anatase TiO_2 are manipulated using salts that contain various species of alkali metal ions in the hydrothermal process.

Needle-shaped anatase TiO_2 (N2-TiO_2) with {301} exposed at its ends and {100} exposed along its body was also synthesized to investigate the photocatalytic behaviors of various planes.[20] Fig. 9A displays a needle shaped particle (N2-TiO_2) with a smooth lateral face. The {100}-exposed face of the N2-TiO_2 body can be determined from the Fourier-transformed image and the angle between the (001) planes and the edge of the needle is 90°, as presented in Fig. 9B. The {301}-exposed face at the ends of N2-TiO_2 can be determined from the angle between the (001) planes and the edge of the needle, which is 82.5°, as shown in Fig. 9C and D.

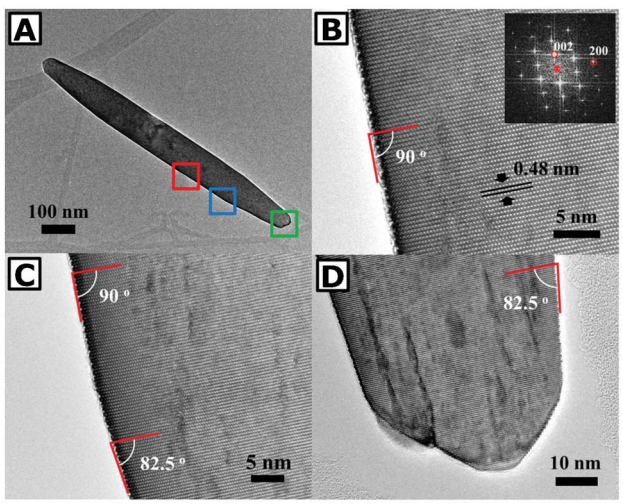

Fig. 9 TEM analyses of N2-TiO_2: (A) TEM image. HRTEM images of region in (B) red, (C) blue and (D) green squares in (A). Inset in (B) displays Fourier-transformed image of N2-TiO_2 body.

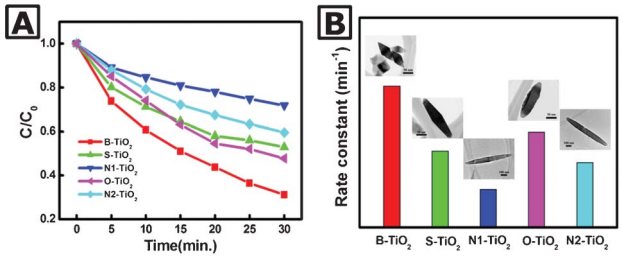

Fig. 10 (A) Photocatalytic performance and (B) calculated rate constants of different anatase TiO_2 in degradation of methylene blue under irradiation.

To understand the relationship between the crystal face and the photocatalytic performance, the photocatalytic behavior of different anatases was studied in the degradation of methylene blue under irradiation from a Xe lamp. B-TiO_2 and S-TiO_2 are {101} (*ca.* 99.8%) and {301}-exposed (*ca.* 95.6%) anatase TiO_2, respectively. N2-TiO_2 has {301} exposed (*ca.* 38.7%) at both ends and {100} exposed (*ca.* 59.6%) body. N1-TiO_2 has {301} exposed (*ca.* 47.8%) at its end, but no preferentially exposed surface along its body. O-TiO_2 has {101} exposed (*ca.* 35.5%) at its ends, but no preferentially exposed surface along its body, as shown in Scheme S1, ESI.† Fig. 10 presents the photodegradation diagram of all TiO_2 samples and Fig. S3, ESI,† shows the photocatalytic performance of commercial P25. Table 1 presents the photodegradation rate constants, the exposed faces and surface areas of TiO_2. The rate constants of B-TiO_2 and S-TiO_2 with similar surface area, but different exposed faces {101} and {301} were 0.037 and 0.020 min^{-1}, respectively. These results strongly suggest that the photoactivity of anatase {101} planes is larger than that of {301} planes. Thus, the {101} plane was exposed at the ends of O-TiO_2 with the addition of LiCl in the reaction, whereas the exposed face of N1-TiO_2 was {301}. The estimated rate constant of O-TiO_2 is larger than that of N1-TiO_2, also indicating that the photoactivity of {101} exceeded that of {301}, as expected. N1-TiO_2 and N2-TiO_2 had similar shapes and sizes. N2-TiO_2 with {100} exposed planes along its body had a higher photodegradation rate constant than did N1-TiO_2. This observation demonstrates that the photoactivities of

Table 1 Calculated rate constant in degradation of methylene blue, exposed faces and surface area of different forms anatase TiO_2

	Rate constant (min^{-1})	Top	Body	Surface area ($m^2\ g^{-1}$)
B-TiO_2	0.037	{101}	{101}	26.29
S-TiO_2	0.020	{301}	{301}	23.17
N1-TiO_2	0.010	{301}	[a]	8.39
O-TiO_2	0.025	{101}	[a]	12.36
N2-TiO_2	0.017	{301}	{100}	7.97

[a] No preferentially exposed surface along its body.

the {100} planes were greater than those nonspecific exposed planes.

Conclusions

In summary, shape-tailored TiO_2 was synthesized by a hydrothermal process using sodium titanate as the precursor in solutions that contained different alkali metal salts. As the atomic number of the alkali metal ion in the solution increased, the grains of anatase that were formed became longer and the shape of the TiO_2 changed. Bipyramidal, spindle-shaped and needle-like TiO_2 powders were obtained in solutions with LiCl, NaCl and KCl additives, respectively. Bipyramidal crystals had exposed {101} planes; spindle-shaped powder had mainly exposed {301} planes, and N1-TiO_2 with a <001> long axis also had exposed {301} planes at both ends. The {301}-exposed anatase TiO_2 is reported upon here for the first time. As is generally known, specific crystal growth of anatase TiO_2 results from the anisotropic stacking of basis planes {100} and {001}. Alkali metals with large charge density were attracted to both {100} and {001} planes, restraining the growth along the related directions, which leads to the growth of small particles with a low aspect ratio, whereas cations with a low charge density cation tended to be absorbed only on the {100} planes, producing particles with a high aspect ratio. These observations also reveal that the restraint of crystal growth follows the order $Li^+ > Na^+ > K^+$. With respect to photocatalytic performance, the results suggest that the {101} facet is highly active in the photodegradation of methylene blue. This work provides a green strategy (organic-free) for synthesizing shape and exposed face tailored anatase TiO_2. The synthetic method may be extensively utilized in the synthesis of various metal oxides with specific shapes and exposed faces, and is expected to perform well in various applications, such as hydrogen generation,[30] dye-sensitized solar cells[6] and the photoreduction of greenhouse gases.[31]

Notes and references

1 G. Liu, J. C. Yu, G. Q. Lu and H.-M. Cheng, *Chem. Commun.*, 2011, **47**, 6763–6783.
2 A. Vittadini, A. Selloni, F. P. Rotzinger and M. Grätzel, *Phys. Rev. Lett.*, 1998, **81**, 2954–2957.
3 C.-W. Peng, T.-Y. Ke, L. Brohan, M. Richard-Plouet, J.-C. Huang, E. Puzenat, H.-T. Chiu and C.-Y. Lee, *Chem. Mater.*, 2008, **20**, 2426–2428.
4 E. S. Jang, J.-H. Won, S.-J. Hwang and J.-H. Choy, *Adv. Mater.*, 2006, **18**, 3309–3312.
5 X. Han, M. Jin, S. Xie, Q. Kuang, Z. Jiang, Y. Jiang, Z. Xie and L. Zheng, *Angew. Chem., Int. Ed.*, 2009, **48**, 9180–9183.
6 X. Wu, Z. Chen, G. Q. Lu and L. Wang, *Adv. Funct. Mater.*, 2011, **21**, 4167–4172.
7 J. S. Chen, Y. L. Tan, C. M. Li, Y. L. Cheah, D. Luan, S. Madhavi, F. Y. C. Boey, L. A. Archer and X. W. Lou, *J. Am. Chem. Soc.*, 2010, **132**, 6124–6130.
8 M. H. Yang, T. T. Chen, Y. S. Wang, H. T. Chiu and C. Y. Lee, *J. Mater. Chem.*, 2011, **21**, 18738–18743.
9 T.-Y. Ke, P.-C. Chen, M.-H. Yang, H.-T. Chiu and C.-Y. Lee, *CrystEngComm*, 2011, **13**, 5292–5295.
10 P. C. Chen, M. C. Tsai, H. C. Chen, I. N. Lin, H. S. Sheu, Y. S. Lin, J. G. Duh, H. T. Chiu and C. Y. Lee, *J. Mater. Chem.*, 2012, **22**, 5349–5355.
11 M. Niederberger and G. Garnweitner, *Chem.–Eur. J.*, 2006, **12**, 7282–7302.
12 H. G. Yang, C. H. Sun, S. Z. Qiao, J. Zou, G. Liu, S. C. Smith, H. M. Cheng and G. Q. Lu, *Nature*, 2008, **453**, 638–U634.
13 T. Y. Ke, C. W. Peng, C. Y. Lee, H. T. Chiu and H. S. Sheu, *CrystEngComm*, 2009, **11**, 1691–1695.
14 L. Wu, B. Yang, X. Yang, Z. G. Chen, Z. Li, H. Zhao, X.-Q. Gong and H. Yang, *CrystEngComm*, 2013, DOI: 10.1039/C2CE26744F.
15 C.-T. Dinh, T.-D. Nguyen, F. Kleitz and T.-O. Do, *ACS Nano*, 2009, **3**, 3737–3743.
16 H. Zhang, Y. Wang, P. Liu, Y. Han, X. Yao, J. Zou, H. Cheng and H. Zhao, *ACS Appl. Mater. Interfaces*, 2011, **3**, 2472–2478.
17 H. B. Jiang, Q. Cuan, C. Z. Wen, J. Xing, D. Wu, X.-Q. Gong, C. Li and H. G. Yang, *Angew. Chem., Int. Ed.*, 2011, **50**, 3764–3768.
18 H. B. Wu, J. S. Chen, X. W. Lou and H. H. Hng, *Nanoscale*, 2011, **3**, 4082–4084.
19 T. Kasuga, M. Hiramatsu, A. Hoson, T. Sekino and K. Niihara, *Langmuir*, 1998, **14**, 3160–3163.
20 J. Li and D. Xu, *Chem. Commun.*, 2010, **46**, 2301–2303.
21 J. Li, Y. Yu, Q. Chen, J. Li and D. Xu, *Cryst. Growth Des.*, 2010, **10**, 2111–2115.
22 A. Chemseddine and T. Moritz, *Eur. J. Inorg. Chem.*, 1999, 235–245.
23 L. W. Yin, Y. Bando, J. H. Zhan, M. S. Li and D. Golberg, *Adv. Mater.*, 2005, **17**, 1972–1977.
24 P.-C. Chen, M.-C. Tsai, Y.-J. Huang, H.-T. Chiu and C.-Y. Lee, *CrystEngComm*, 2012, **14**, 1990–1993.
25 W. Kaminsky, *J. Appl. Crystallogr.*, 2007, **40**, 382–385.
26 R. D. Shannon, *Acta Crystallogr., Sect. A: Cryst. Phys., Diffr., Theor. Gen. Crystallogr.*, 1976, **32**, 751–767.
27 P. D. Cozzoli, A. Kornowski and H. Weller, *J. Am. Chem. Soc.*, 2003, **125**, 14539–14548.
28 N. Murakami, Y. Kurihara, T. Tsubota and T. Ohno, *J. Phys. Chem. C*, 2009, **113**, 3062–3069.
29 H. G. Yang, G. Liu, S. Z. Qiao, C. H. Sun, Y. G. Jin, S. C. Smith, J. Zou, H. M. Cheng and G. Q. Lu, *J. Am. Chem. Soc.*, 2009, **131**, 4078–4083.
30 X. Chen, S. Shen, L. Guo and S. S. Mao, *Chem. Rev.*, 2010, **110**, 6503–6570.
31 W.-N. Wang, W.-J. An, B. Ramalingam, S. Mukherjee, D. M. Niedzwiedzki, S. Gangopadhyay and P. Biswas, *J. Am. Chem. Soc.*, 2012, **134**, 11276–11281.